Measuring kinetic coefficients by molecular dynamics simulation of zone melting

Franck Celestini* and Jean-Marc Debierre
Laboratoire Matériaux et Microélectronique de Provence, Université d'Aix-Marseille III and CNRS, Faculté des Sciences et Techniques de Saint-Jérôme, Case 151, 13397 Marseille Cedex 20, France
(Received 12 November 2001; published 3 April 2002)

Molecular dynamics simulations are performed to measure the kinetic coefficient at the solid-liquid interface in pure gold. Results are obtained for the (111), (100), and (110) orientations. Both Au(100) and Au(110) are in reasonable agreement with the law proposed for collision-limited growth. For Au(111), stacking fault domains form, as first reported by Burke, Broughton, and Gilmer [J. Chem. Phys. **89**, 1030 (1988)]. The consequence on the kinetics of this interface is dramatic: the measured kinetic coefficient is three times smaller than that predicted by collision-limited growth. Finally, crystallization and melting are found to be always asymmetrical and here again the effect is much more pronounced for the (111) orientation.

DOI: 10.1103/PhysRevE.65.041605 PACS number(s): 81.10.−h, 81.30.Fb, 68.08.−p, 02.70.Ns

I. INTRODUCTION

Solidification of pure elements is of technological interest because the way a given material solidifies usually affects its structure and, as a consequence, its final elastic and other macroscopic properties. From a fundamental point of view, interest in free and directed solidification comes from the underlying nonlinear physics, morphological instabilities being at the origin of generic microstructures such as dendrites or cells.

Important theoretical and numerical contributions have been made to solve this difficult physical problem [1]. Recently, a quantitative phase field model was introduced [2]. A subsequent refinement, consisting in solving the diffusion equation with the help of Brownian walkers, permitted to bridge the wide gap between the capillary and diffusion lengths, allowing direct comparison with experiments [3]. As a consequence, there is currently an increasing need for accurate values of the interface response functions that are used as input parameters for realistic phase field simulations.

In the case of a pure element, the surface tension $\gamma_{\measuredangle mn}$ must be known as a function of the interface orientation ($\measuredangle mn$). In addition, the kinetic coefficient $\mu_{\measuredangle mn}(T_i)$ giving the relation between the interface velocity and the interface temperature T_i, should also be known for the different orientations. For a binary alloy, temperature dependence of the solute diffusion coefficient $D(T)$ as well as velocity and orientation dependence of the segregation coefficient $k_{\measuredangle mn}(V_i)$ are also necessary.

Both k and μ are hardly accessible in the experiments and convection effects often lead to overestimated values of diffusion coefficients. Different simulation schemes have thus been proposed as an alternative. Such numerical experiments have been rendered possible by the discovery of realistic interatomic potential models, such as, in the case of metals, the embedded atom model [5], the glue model [4], and the effective medium theory [6]. In the near future, the increase of computer power should open the possibility to address the case of more complicated materials such as semiconductors, molecular crystals, and organic compounds, for which potentials do not simply reduce to pair interactions. Very recently, the functions $\gamma_{\measuredangle mn}$ and $\mu_{\measuredangle mn}(T_i)$ have been determined and used in phase field simulations of dendritic growth for pure nickel [7]. The good quantitative agreement found between experiments and simulations is promising and should stimulate in the near future the construction of other material-dedicated phase field models.

New methods for the determination of the functions $\gamma_{\measuredangle mn}$ and $k_{\measuredangle mn}(V_i)$ have been recently proposed [8,9]. In the present paper, we rather concentrate on $\mu_{\measuredangle mn}(T_i)$. The kinetic response of a solid-liquid interface has been simulated quantitatively in the 80's by Broughton, Gilmer, and Jackson (BGJ) for a Lennard-Jones (LJ) potential and a (100) orientation [10]. These authors showed that growth is *not* diffusion limited but rather that the interface velocity is related to the mean kinetic energy of the atoms. For this collision-limited growth regime, the growth rate should be directly proportional to the distance between two successive layers $d_{\measuredangle mn}$. Indeed, since the liquid atoms do not diffuse to choose their adsorption sites but are almost instantaneously incorporated into the solid, the larger $d_{\measuredangle mn}$ the more effective and the faster the advance of the solid-liquid interface should be. The analytical expression for the growth velocity of a rough solid-liquid interface reads [11]

$$V \propto d_{\measuredangle mn} \tilde{V} \left[1 - \exp\left(- \frac{\Delta \tilde{\mu}}{kT} \right) \right], \tag{1}$$

$d_{\measuredangle mn}$ being the interplane spacing, $\Delta\tilde{\mu}$ the chemical potential difference between solid and liquid phases, T the absolute temperature, k the Boltzmann constant, and $\tilde{V}$ the thermal velocity. This law is confirmed by molecular dynamics (MD) simulations for the (100) and (110) orientations: the expected $\sqrt{2}$ ratio between the corresponding kinetic coefficients is well recovered for several metals crystalizing in a face centered cubic (fcc) structure (Ni, Ag, and Au) [12,13]. Nevertheless, for these rough materials, growth of the (111) interface does not obey this simple law: according to Eq. (1), the (111) orientation should be much faster, and what is found is precisely the opposite. Burke, Broughton, and

*Electronic address: celest@12mp.u-3mrs.fr

Gilmer [11] attribute this slowing down to the growth of competing fcc and hcp domains in the solidifying layer, followed by the elimination of the defect lines between the two phases.

Another question associated with solid-liquid interfaces is that of symmetry between solidification and melting kinetics. Asymmetry has been already observed in different systems. It is not really surprising for faceted materials such as silicium where solidification involves nucleation while melting does not. The question is more delicate when one considers rough materials with collision-limited growth. Indeed, available results are controversial: if asymmetry has been found for a Na(100) interface [14], it has not been observed for a LJ(100) [15]. More surprisingly, in the latter case an opposite asymmetry (crystal growing faster than the melt) can be found, depending on the way the solid germ is prepared.

In this paper, we address the above questions concerning the growth of a rough solid-liquid interface. We first present our implementation of a nonequilibrium molecular dynamics scheme for a zone melting experiment. Section II is devoted to the study of (100) and (110) orientations. The special case of (111) growth is examined in Sec. III and asymmetry between melting and solidification in Sec. IV. Finally, a summary of the different results and a discussion are given in the Sec. VI.

II. SIMULATION PROCEDURE

For this study we use the Ercolessi glue potential for Au [4]. In this formalism the total potential energy for a system of N atoms is given by

$$U=\frac{1}{2}\sum_{i,j=1}^{N}\Phi(r_{ij})+\sum_{i=1}^{N}U(n_i). \tag{2}$$

The first term is a classical pair interaction. In the second term, n_i is the coordination of atom i,

$$n_i=\sum_{j=1}^{N}\rho(r_{ij}), \tag{3}$$

where $\rho(r_{ij})$ is a function of the interatomic distance r_{ij}, with a cutoff radius of 3.9 Å here. The energy function U is the *glue term* associating an extra potential energy to atom i as a function of its coordination. This glue potential has demonstrated its efficiency in predicting the physical properties of gold as well as in describing several experimentally observed phenomena such as surface melting and surface reconstructions [16].

A distinctive feature of our method is to simulate a zone melting experiment in which both a solidification and a melting front are simultaneously advancing at a fixed velocity V. This velocity is that of the virtual furnace that imposes two symmetric thermal gradients. The particle coordinates are defined in a reference frame moving at velocity V in the z direction, so that after equilibration the positions of the two interfaces are fixed in the simulation box. Heat transport from the furnace is simulated by imposing one temperature below and one above the melting point inside two distant slices, 20 Å each in thickness (Fig. 1). Within each slice, temperature is kept constant by using a classical velocity rescaling procedure [17]. Periodic boundary conditions are applied in the three directions. More details about the numerical method can be found in a recent study of solute trapping in a LJ binary alloy, where a similar simulation technique was used [9].

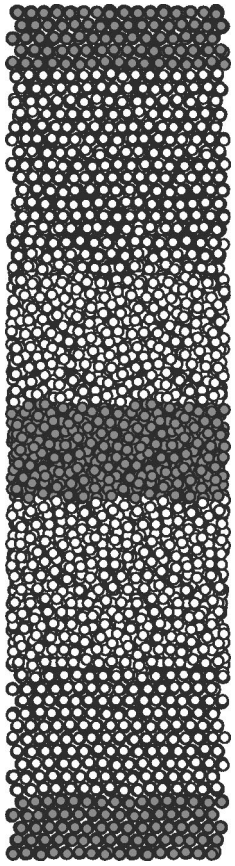

FIG. 1. A typical simulation box with periodic boundary conditions in all three directions [(111) solid-liquid interfaces]. Atoms in dark gray are within the hot and cold slices where temperature is fixed.

First, the fcc solid and the liquid are equilibrated separately at zero pressure and at a temperature close of the melting point. Our smallest system has a size $S_0 \simeq 20\times 20$ Å^2 in cross section, that is about 64 atoms per layer. After equilibration, the solid and liquid are brought into contact and plunged in the temperature gradient imposed by the two temperature-controlled slices. The total system is about 220 Å in height. After a second equilibration period (during which the velocity of the furnace is zero), the two interfaces reach a stationary position and we roughly have 50% of solid and liquid (see Fig. 1). Figure 2 shows the temperature and energy profiles along the z axis.

Combining the two profiles to eliminate the z coordinate, one obtains a caloric curve, i.e., a plot of energy as a function of temperature. In Fig. 3, the caloric curves obtained for two different values of the pulling velocity V are displayed. For $V=0$, the data points corresponding to the solidification and the melting fronts merge onto the same curve: no kinetic

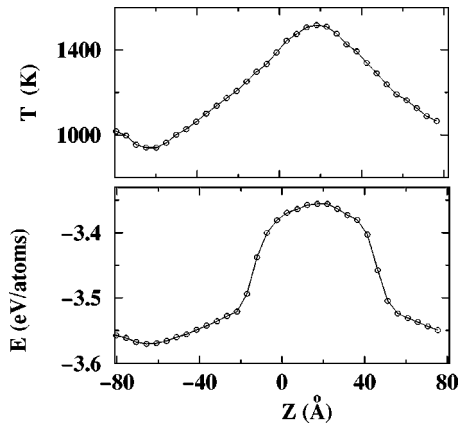

FIG. 2. Temperature and energy profiles along the *z* axis perpendicular to the interfaces.

effects are at play and the interface temperature is the equilibrium melting temperature $T_0 \simeq 1330$ K. When a velocity is imposed, a dynamical hysteresis appears on the caloric curve. Kinetic effects split the curve in two distinct parts: the interface temperature of the solidification front decreases while it increases on the melting front. We can deduce both interface undercooling and interface superheating from this plot. An interest of this method is that, as said before, the interface is fixed in the reference frame of the simulation box, so that statistics are easy to record. A typical run lasts 10^6 MD steps (3.5×10^3 ps), so that the atoms in the system solidify and melt several times. According to a recent study by Tepper and Briels [15], we know that the melting kinetics can be affected by the way the solid is equilibrated. Thus multicycling is necessary to mimic the melting of a real solid, usually resulting from previous solidification(s).

To conclude this section, the method used to estimate the interface temperature T_i from the caloric curves is described. We assume the energy of atoms lying at the interface, E_i, to be a weighted average of the perfect solid and liquid energies at the same temperature T,

$$E_i(T) = \alpha E_S(T_{-i}) + (1-\alpha) E_L(T_{-i}). \tag{4}$$

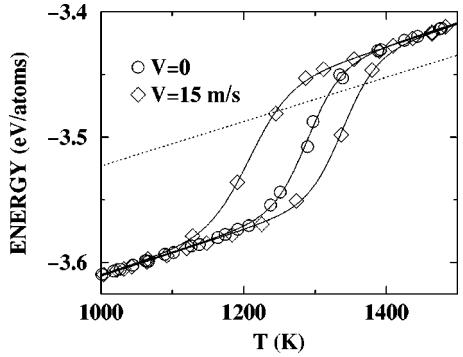

FIG. 3. Caloric curves for $V=0$ (circles) and $V=15$ ms^{-1} (diamonds). For nonzero velocity, the kinetic effects split the curve into two parts. The dotted straight line represents the function $E_i(T)$.

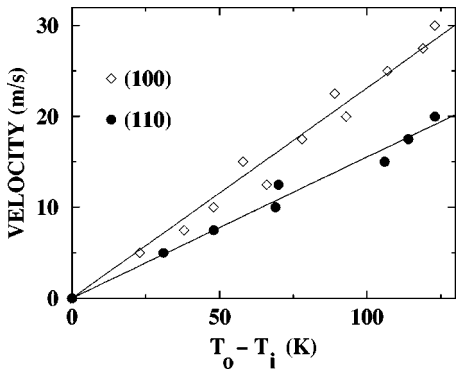

FIG. 4. Velocity of the solid-liquid interface as a function of undercooling for (100) and (110) orientations. The straight lines are best fits to a linear kinetic law.

Linear relations, $E_S(T) = a_S T + b_S$, and $E_L(T) = a_L T + b_L$, are fitted to the data points obtained on the low and high temperature side, respectively (Fig. 3). The curve $E_i(T)$ is thus a line with a slope

$$p = \alpha a_S + (1-\alpha) a_L. \tag{5}$$

The value of coefficient α is then extracted from the caloric curve at zero velocity, for which T_i must be equal to T_0 (Fig. 3). Finally, the interface temperature is given by the intersection of the line $E_i(T)$ with the caloric curve. An alternative method consists in building an order parameter that distinguishes between solid and liquid atoms [8,18]: a plot of this order parameter as a function of temperature also gives an interface temperature. We have checked that the two methods give equivalent results.

III. GROWTH OF (100) AND (110) INTERFACES

In this section we compute the kinetic coefficient for the Au(100) and Au(110) interfaces, using the method described above. We concentrate here on pulling velocities ranging between $V=5$ m s^{-1} and $V=30$ m s^{-1}, for which kinetics remain linear. We also perform a few simulations at higher velocities, where kinetics deviates from linearity, but comments on nonlinear effects are postponed to the concluding section. In Fig. 4, we plot the interface velocity as a function of the measured undercooling $T_0 - T_i$. Linear fits to the law

$$V = \mu_{\nearrow mn}(T_0 - T_i) \tag{6}$$

give the following estimates for the two kinetic coefficients:

$$\mu^{\star}_{100} = 23.1 \pm 1.0 \ \text{cm s}^{-1}\,\text{K}^{-1} \tag{7}$$

and

$$\mu^{\star}_{110} = 15.5 \pm 1.0 \ \text{cm s}^{-1}\,\text{K}^{-1}. \tag{8}$$

However, finite-size effects are expected to bias these estimates because the system cross-section area, $S_0 = 20 \times 20$ Å^2, is rather small.

Additional runs are thus performed in order to quantitatively evaluate finite-size effects. The pulling velocity is

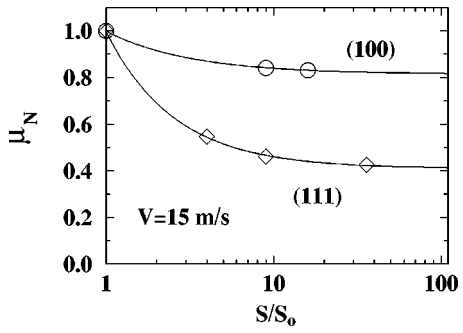

FIG. 5. Normalized kinetic coefficient as a function of system size S for the (100) and (111) orientations.

fixed to $V=15\ \mathrm{m\,s^{-1}}$, the system height to $H\simeq 222$ Å, and the cross-section area S is progressively increased. We define the normalized kinetic coefficient $\mu_N(S)$ as the ratio of the kinetic coefficient obtained at size S to that obtained at size $S=S_0$ [Eqs. (7)–(8)]. As shown in Fig. 5, the size effects are important and the kinetic coefficients appear to converge only for $S\simeq 100\times 100$ Å^2. For the (100) direction, there is a decrease of about 20% and we obtain roughly the same behavior for the (110) interface. This size effect has never been reported in the past for (100) and (110) orientations: the fact that Hoyt and co-workers do no find size effects for these two orientations [8] is certainly due to the fact that their smaller system is larger than ours. We can now propose extrapolated values for the kinetic coefficients:

$$\mu_{100}=18.8\pm 1.0\ \ \mathrm{cm\,s^{-1}\,K^{-1}}, \tag{9}$$

$$\mu_{110}=12.6\pm 1.0\ \ \mathrm{cm\,s^{-1}\,K^{-1}}. \tag{10}$$

The corresponding ratio $\mu_{100}/\mu_{110}=1.49\pm 0.15$ is in good agreement with the value $\sqrt{2}$ predicted by Eq. (1). Hence, the assumption of collision-limited growth for (100) and (110) orientations is confirmed to be the relevant one. At this point, we can compare our results with those of Hoyt *et al.* for gold [13]. If they also find a $\sqrt{2}$ ratio between their two orientations, their μ values are larger than ours by a factor 1.8. Linearizing the expression given by BGJ, we find

$$V\sim T_0^{-1}T_i^{-1/2}(T_0-T_i) \tag{11}$$

for the interface velocity. The potential used by Hoyt *et al.* gives a melting point T_0 of 1090 K [19] much smaller than the value 1330 K obtained with Eroclessi potential. Introducing this temperature shift in Eq. (11) roughly accounts for the discrepancy between the values of μ. Since Ercolessi potential gives a melting point much closer to the experimental one, it should be also the case for our estimates of the kinetic coefficients.

In order to understand the origin of the size effects on the value of the kinetic coefficient, we take now a closer look at the in-plane structure of gold layers in the vicinity of the solid-liquid interface. We compute a density profile along the z axis from which we are able to separate atoms belonging to different layers. Deep in the solid the in-plane square structure of the (100) orientation is effectively recovered without any significant amount of defaults and vacancies. For the two solid layers just below the interface the situation is more complex. To distinguish between different symmetries, we first perform a Voronoi construction [20] for all the atoms in the layer. We then collect the set of first neighbors for each atom.

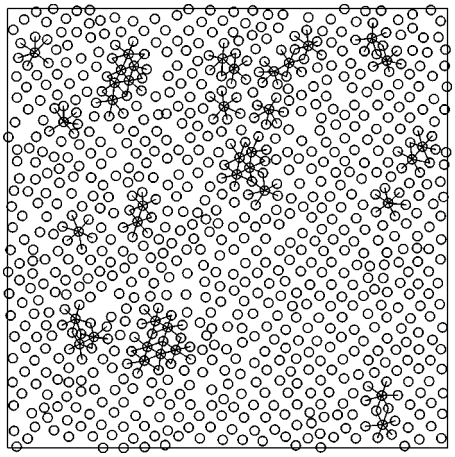

FIG. 6. Snapshot showing the atoms in the (100) solid layer next to the interface. The Delaunay triangulation is only drawn in regions with triangular underlying symmetry.

For a fcc solid with lattice parameter a, on the square lattice of the (100) orientation an atom has four nearest neighbors at a distance $a/\sqrt{2}$ and four second nearest neighbors at a distance a. On the other hand, for a triangular lattice [as the one of the (111) plane] the six neighbors all lie at the same distance $a/\sqrt{2}$. In Fig. 6, we show a snapshot of the interface solid layer where the Delaunay triangulation is only drawn for the atoms that have six first neighbors at comparable distances, in order to reveal the local triangular structure. It is clear that most of the atoms have reached their positions on the square lattice but several islands with a triangular symmetry remain. Note that the number of atoms in the layer has already attained the value it will have deep in the solid with a perfect square structure. To compensate for the higher density of the triangular structure, the corresponding islands are surrounded by a border region where the density is very low. This coexistence of two symmetries is not observed in our smallest system: one can imagine that for a small area the square structure is easily formed and hence triangular islands do not appear. This phenomenon is very close to the well known reconstruction of the (100) solid-vapor interface where the first layer adopts a triangular structure [21]. Turning back to the solid-liquid interface, the system apparently uses some of the solidification driving force to eliminate one of the two phases and finally reach an almost perfect square symmetry. Hence, the interface velocity is lower for larger systems.

Such an in-plane ordering is not taken into account in the collision-limited model but in spite of this we recover the predicted $\sqrt{2}$ value for the ratio μ_{100}/μ_{110}. This suggests a similar effect, roughly of the same order, for the (110) orientation. We have not been able to visualize ordering at (110)

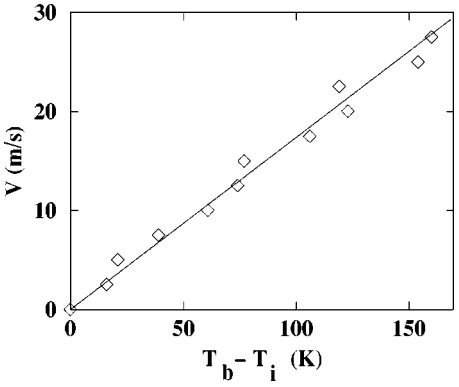

FIG. 7. Velocity of the (111) solid-liquid interface as a function of undercooling.

interfaces but one could imagine a mechanism reminiscent of the missing row reconstruction observed for (110) solid-vapor interfaces.

IV. THE SPECIAL CASE OF (111) INTERFACE

We now turn to the case of the (111) orientation. In the same way as above for the (100) and (110) orientations we calculate the interface temperature for different velocities. As can be seen in Fig. 7, a linear kinetic law is also valid for the (111) orientation. Results of the finite-size analysis, presented in Fig. 5, show that the size effects are much more pronounced than for the (100) orientation. The extrapolated value of the kinetic coefficient,

$$\mu_{111} = 7.0 \pm 1.0 \ \ \mathrm{cm\,s^{-1}\,K^{-1}}, \tag{12}$$

is now 60% below its value for $S = S_0$. Relatively to the two other orientations, we find

$$\mu_{111} \simeq 0.37 \mu_{100} \simeq 0.56 \mu_{110}. \tag{13}$$

These ratios largely differ from the values predicted by Eq. (1), respectively, $2/\sqrt{3} \simeq 1.15$ and $2\sqrt{2/3} \simeq 1.63$. The (111) orientation, expected to grow faster because of a larger interlayer spacing, is surprisingly found to be the slowest one. This discrepancy tells us that the growth mechanism for the (111) orientation is not, or at least not only, a collision-limited one.

Here again we look at the symmetries inside the layers close to the interface. For a (111) layer, there are three possible ordered phases lying on three different but equivalent sublattices that we will call *a*, *b*, and *c*. As the stacking fault energy is weak for gold (it is actually zero for the potential we use), once a perfect, say *a*, layer is formed, the next layer to form is either *b* or *c*. In Fig. 8, we show a snapshot of the three uppermost solid layers and we distinguish between atoms belonging to *a*, *b*, or *c* phases. For the lowest solid layer, phase *a* is selected and it occupies the whole plane. For the layer just above, there is coexistence between *b* and *c* sublattices. Finally, in the highest solid layer, all three phases coexist. We recover here the effect first observed by Burke *et al.* [11] for a LJ potential. For a (111) orientation the system hesitates between the different phases it can equivalently

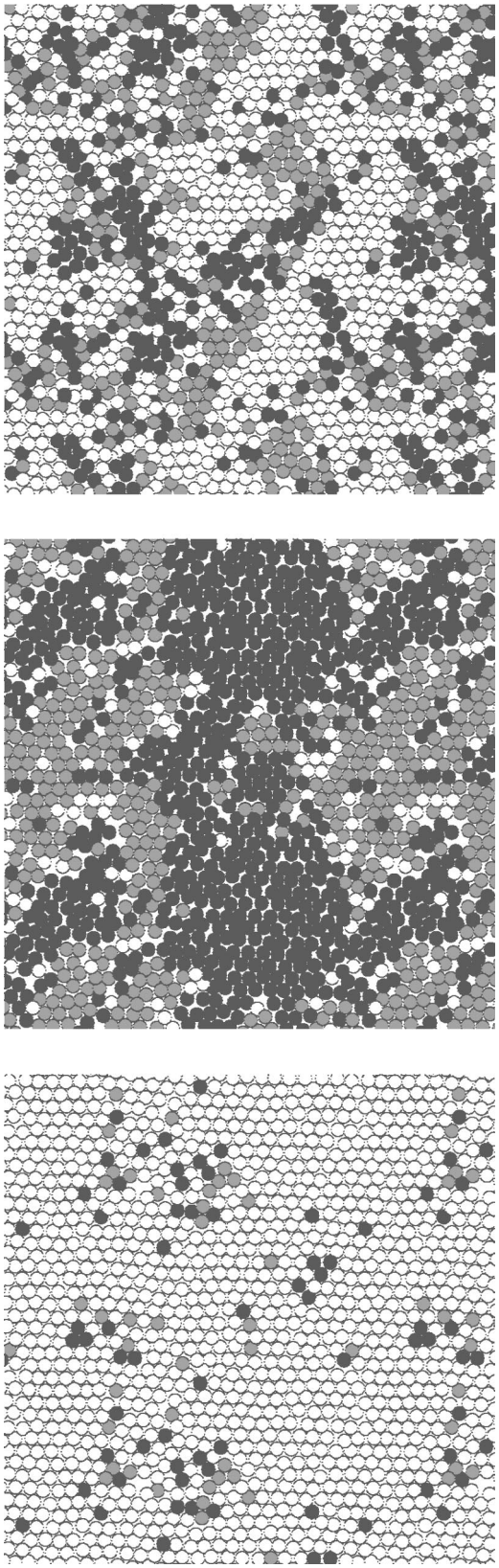

FIG. 8. Snapshots of the three solid layers immediately below the interface (top layer in contact with the liquid phase). The gray levels correspond to the three different sublattices: *a* (white), *b* (light gray), c (dark gray).

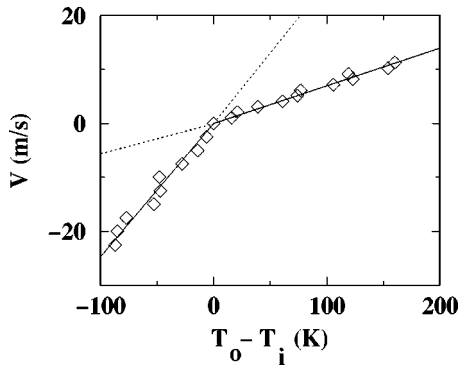

FIG. 9. Velocity of the (111) solidification and melting interfaces as a function of undercooling. Note that the results for solidification incorporate finite-size corrections.

form. Here again, the system dissipates a part of the available driving force to select one of the phases. As a consequence, the velocity of the interface is reduced as compared to the value expected for a purely collision-limited growth. The size effect is easily understood because in a small system, coexistence is strongly reduced. It would be of interest to determine the amount of driving force spent in this in-plane organization in order to estimate the corresponding decrease in V_{111}. To perform this, one could for instance use a three-state Potts model in three dimensions with ferromagnetic intraplane and antiferromagnetic interplane interactions. To conclude this section we have to point out that phase coexistence is related to the value of the stacking fault energy E_s. For a material with large E_s phase coexistence should be less probable and the front velocity in better agreement with the prediction of Eq. (1).

V. ASYMMETRY BETWEEN MELTING AND SOLIDIFICATION

As discussed in the Introduction, asymmetry is obvious for faceted materials but is not as clear when considering rough materials such as metals. The question is to know if, at equal absolute undercooling and superheating, the solid-liquid and liquid-solid fronts have the same velocity. With our simulation scheme, this study is straightforward, since both a melting and a solidification fronts are simulated at once: no additional calculations are thus required. Figure 9 represents the velocities of both the melting and solidification fronts as functions of $T_0 - T_i$ for the (111) orientation (in our conventions a positive velocity corresponds to solidification). The data are obtained in a system of size $S = S_0$ and corrected according to the finite-size analysis reported above. It is important to note that no size effects are actually found for the melting front: in contrast with the solidification front, the melting interface temperature remains the same whatever the system size. This can be understood if one remembers that for solidification, especially for the (111) orientation, growth is not only collision limited but also requires in-plane ordering. This is no longer the case for melting, which justifies the absence of size effects. The asymmetry shown in Fig. 9 is larger for the (111) orientation. The same analysis is also made for the two other orientations and we find the following degrees of asymmetry:

$$\mu^m_{111} = 25 \pm 4 \ \ \mathrm{cm\,s^{-1}\,K^{-1}} \simeq 3.6 \mu^s_{111}, \tag{14}$$

$$\mu^m_{100} = 39 \pm 2 \ \ \mathrm{cm\,s^{-1}\,K^{-1}} \simeq 2.1 \mu^s_{100}, \tag{15}$$

$$\mu^m_{110} = 20 \pm 2 \ \ \mathrm{cm\,s^{-1}\,K^{-1}} \simeq 1.6 \mu^s_{110}, \tag{16}$$

where the superscripts *s* and *m* refer, respectively, to solidification and melting kinetics. An asymmetry is revealed in the three cases but it is more pronounced for the (111) orientation in the same way as size effects observed during solidification. We conclude here that this asymmetry is directly related to the ordering within the interface layers. The asymmetry is strong for (111) because of the peculiar growth mechanism discussed in the preceding section.

The melting front is found to be faster than the solidification interface in agreement with the idea that disordering is an easier task than ordering. Our results confirm the majority of experimental and numerical studies [14,22–25]. We also confirm the conclusions of a debate between Richards [26] and Oxtoby and co-workers [27,28] on the importance of density change on the asymmetry between melting and solidification kinetics. In agreement with the conclusions of Oxtoby, the gold density change at melting is small ($\simeq$2%) and can not be responsible for such an important asymmetry. On another hand, Tepper [15] does not find asymmetry for the growth of a (100) LJ solid. Even if the materials differ, they both belong to the same class of rough materials and such a qualitative difference may be surprising. Nevertheless, one should remember the strong tendency to surface reconstruction in Au, as observed for the (100) orientation where triangularlike regions are formed. This tendency is furthermore enhanced by the use of Ercolessi glue potential but is weaker for a LJ potential, what could explain the different behaviors observed.

Finally, comparing the melting kinetic coefficients in the different orientations, we find $\mu^m_{100} > \mu^m_{111} > \mu^m_{110}$. We presently do not have a satisfactory explanation for this hierarchy in the melting kinetics.

VI. DISCUSSION

Our molecular dynamics simulations of zone melting experiments allow us to measure simultaneously the solidification and melting kinetics for a pure element.

For (100) and (110) orientations, growth is apparently well described by a collision-limited process. Nevertheless, we observe small 2D islands with triangular symmetry to form in the solid layer at the (100) solid-liquid interface. As a consequence, size effects and asymmetry between melting and solidification are found. We cannot decide whether this effect is solely due to the tendency of the glue potential to overestimate surface reconstruction, or if it is an intrinsic property of gold and/or other metals.

The case of the (111) orientation is rather special. Phase coexistence of three triangular sublattices, as first proposed by Burke *et al.* [11], is recovered. This peculiar behavior has

a strong influence on the kinetics of the interface. Our finite-size analysis show that in order to measure a realistic value of the kinetic coefficient one has to simulate systems with a solid-liquid interface area larger than 100×100 Å^2. The consequence on asymmetry between melting and solidification is also of importance: for a given driving force, the melting front is more than three times faster than the solidification one. Because of this disagreement with a purely collision-limited growth, no analytical model seems, at present, able to predict the kinetic law of a (111) interface. As discussed previously, it would be interesting to use a statistical model to extract the amount of driving force spent for phase separation in order to modify Eq. (1) and find an acceptable expression for the interface velocity.

For melting we find the following order between the different kinetic coefficients: $\mu^m_{100}>\mu^m_{111}>\mu^m_{110}$. To our knowledge this hierarchy does not obey any existing law. This result will hopefully stimulate further investigations to reach a clear understanding of the specificities of melt growth as compared to crystal growth.

The present study is devoted to the linear relationship between velocity and undercooling. For all the orientations considered here, nonlinear effects appear at velocity $V\simeq30$ m s^{-1} and undercooling $\Delta T\simeq200$ K. It is not possible to explain this deviation using either the diffusion limited [29,30] or the collision-limited growth law. This suggests a possible change in the interface structure for such large deviations from equilibrium. Density difference between the liquid and solid phases should also contribute to trigger nonlinear behavior [26]. Understanding this crossover would be of importance in the context of very rapid solidification.

Finally, we would like to stress that the kinetic effects can contribute to the anisotropy of the segregation coefficient $k(V)$ for a binary alloy. At sufficiently large velocity, one expects an important difference in the interface temperatures for (111) and (100) orientations. As a consequence, the diffusivity of solvent atoms and hence the segregation coefficient, as predicted by the Aziz law [31], should also differ. This effect may cause solute trapping to appear at lower velocities for (111) than for (100) or (110) orientations. We are currently investigating such segregation effects induced by kinetic anisotropy in the Al-Cu system.

ACKNOWLEDGMENTS

It is a pleasure for us to thank M. Asta, B. Billia, J. J. Hoyt, and A. Karma for fruitful discussions.

[1] K. Kassner, *Pattern Formation in Diffusion-Limited Crystal Growth* (World Scientific, Singapore, 1996).
[2] A. Karma and W. J. Rappel, Phys. Rev. E **57**, 4323 (1998).
[3] M. Plapp and A. Karma, Phys. Rev. Lett. **84**, 1740 (2000).
[4] F. Ercolessi, M. Parrinello, and E. Tossati, Philos. Mag. A **58**, 213 (1988).
[5] M. S. Daw and M. I. Baskes, Phys. Rev. B **29**, 6443 (1984).
[6] K. W. Jacobsen, J. K. Nørskov, and M. J. Puska, Phys. Rev. B **35**, 7423 (1987).
[7] J. Bragard, A. Karma, Y. H. Lee, and M. Plapp, Int. Sci. (to be published).
[8] J. J. Hoyt, M. Asta, and A. Karma, Phys. Rev. Lett. **96**, 5530 (2001).
[9] F. Celestini and J. M. Debierre, Phys. Rev. B **62**, 14 006 (2000).
[10] J. Q. Broughton, G. H. Gilmer, and K. A. Jackson, Phys. Rev. Lett. **49**, 1496 (1982).
[11] E. Burke, J. Q. Broughton, and G. H. Gilmer, J. Chem. Phys. **89**, 1030 (1988).
[12] J. J. Hoyt, B. Sadigh, M. Asta, and S. M. Foiles, Acta Mater. **47**, 3181 (1999).
[13] J. J. Hoyt, M. Asta, and A. Karma (private communication).
[14] J. Tymczak and J. R. Ray, Phys. Rev. Lett. **64**, 1278 (1990); J. Chem. Phys. **92**, 7520 (1990).
[15] H. L. Tepper and W. J. Briels, J. Cryst. Growth **230**, 270 (2001).
[16] F. Ercolessi, A. Bartolini, M. Garofalo, M. Parrinello, and E. Tosatti, Surf. Sci. **189**, 55 (1989); F. Ercolessi, S. Iarlori, O. Tomagnini, E. Tosatti, and X. J. Chen, *ibid.* **251**, 951 (1991).
[17] M. P. Allen and D. J. Tildesley, *Computer Simulation of Liquids* (Clarendon Press, Oxford, 1987).
[18] W. J. Briels and H. L. Tepper, Phys. Rev. Lett. **79**, 5074 (1997).
[19] S. M. Foiles and J. B. Adams, Phys. Rev. B **40**, 5909 (1989).
[20] F. F. Preparata and M. L. Shamos, *Computational Geometry: An Introduction* (Springer, New York, 1985).
[21] D. Passerone, Ph.D. thesis, SiSSA-ISAS 1998.
[22] M. D. Kluge and J. R. Ray, Phys. Rev. B **39**, 1738 (1989).
[23] J. Y. Tsao, M. J. Aziz, M. O. Thompson, and P. S. Peercy, Phys. Rev. Lett. **56**, 2712 (1986).
[24] R. Moss and P. Harrowell, J. Chem. Phys. **100**, 7630 (1994).
[25] G. H. Rodway and J. D. Hunt, J. Cryst. Growth **112**, 554 (1991).
[26] P. M. Richards, Phys. Rev. B **38**, 2727 (1988).
[27] D. W. Oxtoby and P. R. Harrowell, J. Chem. Phys. **96**, 3834 (1991).
[28] Y. C. Shen and D. W. Oxtoby, J. Chem. Phys. **104**, 4233 (1996).
[29] H. A. Wilson, Philos. Mag. **50**, 238 (1900).
[30] J. Frenkel, Phys. Z. Sowjetunion **1**, 498 (1932).
[31] M. J. Aziz, J. Appl. Phys. **53**, 1158 (1981).